ORIGINAL SCIENTIFIC PAPER

CROATICA CHEMICA ACTA

Croat. Chem. Acta **2018**, *91*(3)
Published online: September 24, 2018
DOI: 10.5562/cca3316

HKD 1926

Synthesis, Quantum Chemical Calculations and Molecular Docking Studies, Biological and Anion Sensor Properties of (*E*)-4-[(4-ethoxy-phenylimino)methyl]-2-methoxyphenol

Celal Tuğrul Zeyrek[1], Hüseyin Ünver[2], Bahadir Boyacioglu[3], Neslihan Demir[4], Gönül Yapar[5], Hakan Dal[6], Mustafa Yıldız[7,*]

[1] Ankara Nuclear Research and Training Center, Turkish Atomic Energy Authority, TR-06100 Besevler-Ankara, Turkey
[2] Department of Physics, Faculty of Science, University of Ankara, TR-06100 Besevler- Ankara, Turkey
[3] Vocational School of Health Services, Ankara University, TR-06290 Kecioren-Ankara, Turkey
[4] Department of Biology, Faculty of Arts and Sciences, Çanakkale Onsekiz Mart University, TR-17100 Çanakkale, Turkey
[5] Department of Chemistry, Faculty of Arts and Sciences, Istanbul Technical University, TR- 34469 Istanbul, Turkey
[6] Department of Chemistry, Faculty of Science, Anadolu University, TR-26470 Yenibağlar, Eskişehir, Turkey
[7] Department of Chemistry, Faculty of Sciences and Arts, Çanakkale Onsekiz Mart University, TR-17100 Çanakkale, Turkey
* Corresponding author's e-mail address: myildiz@comu.edu.tr

RECEIVED: February 20, 2018 * REVISED: July 5, 2018 * ACCEPTED: July 25, 2018

Abstract: We report the synthesis and characterization, biological activity, DNA binding, colorimetric anion sensor properties, computational (HF) and molecular docking studies of a novel Schiff base (*E*)-4-[(4-ethoxyphenylimino)methyl]-2-methoxyphenol. The molecular structure of the title compound was experimentally determined using spectroscopic data and was compared to the structure predicted by theoretical calculations using density functional theory (DFT). In addition, atomic charges, molecular electrostatic potential (MEP), nonlinear optical (NLO) effects, the potential energy surface (PES) scans about two important torsion angles and thermodynamic properties of the title compound were predicted using DFT. The antimicrobial activity of the compound was investigated for minimum inhibitory concentration. UV-Vis spectroscopy studies of the interactions between the compound and calf thymus DNA (CT-DNA) showed that the compound interacts with CT-DNA via intercalative binding. The colorimetric response of the Schiff base receptors in DMSO was investigated. The most discernable color change in the Schiff base was caused by CN^-, which demonstrated that the ligand can be used to selectively detect CN^-.

Keywords: molecular docking, DFT, anti-microbial activity, DNA binding, anion sensor.

INTRODUCTION

VANILIN (4-hydroxy-3-methoxybenzaldehyde) is a pleasant-smelling aromatic compound, which is the principal flavoring constituent in vanilla beans. As a primary substitute for natural vanilla, vanillin is widely used as an ingredient in food and animal feeds. It serves as a food flavoring, a pharmaceutical intermediate and a fragrance in perfumes and odor-masking -masking products. The Schiff bases of 4-hydroxy-3-methoxy-1-benzaldehyde (vanillin) have been extensively studied because of their important applications.[1–6] They have been used as a fluorescent probes for Ag^+ in aqueous solution.[7] These compounds, as well as their metal complexes, have been found to possess biological activity[8] and were used in DNA binding studies of Mg(II) complex.[9] Antibacterial activity has also been reported for the Co(II), Ni(II), Cu(II) and Zn(II) complex of the Schiff base of 4-hydroxy-3-methoxy- 1-benzaldehyde.[5]

Schiff base ligands may contain a variety of substituents with different electron- donating or electron-withdrawing groups, and therefore may have interesting chemical properties. Besides the biological activity, solid-state thermochromism and photochromism are other characteristics of these compounds leading to their

application in various areas of materials science such as the control and measurement of radiation intensity, display systems and optical memory devices.[10–12] Schiff bases derived from 2-hydroxyaldehydes are excellent models for the study of keto-enol tautomerism both in solution and in the solid state.[13–15]

It has been demonstrated in some studies that Schiff bases and their complexes can be used as sequence specific DNA binding agents, and diagnostic agents in medicinal applications and for genomic research.[16–19]

The colorimetric anion sensors are more important, because such materials are useful since they provide visual information more easily. Some anions are duplicitous, both beneficial and deleterious to human health and the environment.[20] Though cyanide is important in industrial processes, exposure to it is highly toxic and can lead to fatal consequences.[21] Schiff bases have gained prominence as a choice for anion sensors due to their unique characteristics such as easy synthesis through one step condensation, existence of easy-to-manipulate hydrogen bonds,[22,23] deprotonation of the hydroxyl (-OH) group,[24,25] and ability to undergo tautomerism.[26,27]

In this study, the novel bidentate Schiff base was synthesized by the reaction of 4-ethoxyaniline with 3-methoxy-4-hydroxybenzaldehyde. The chemical structure was determined through spectroscopic and crystallographic methods. The Schiff base was investigated for its ability to selectively sense anions, antimicrobial activity and in binding to DNA. Molecular docking was also completed to identify the interaction of the title compound with DNA. Moreover, theoretical and experimental structures were compared using quantum-mechanical calculations.

EXPERIMENTAL

Reagents and Techniques

The ^{1}H-, ^{13}C-NMR spectra were recorded on a Bruker DPX FT-NMR spectrometers operating at 500 and 125.7 MHz C-N-H analyses were performed on a LECO CHNS-932 analyzer. Infrared absorption spectra were obtained from a Perkin Elmer BX II spectrometer in KBr discs. UV-Visible spectra were measured by using a Perkin Elmer Lambda 2 series spectrophotometer with 1.0 cm quartz cells. 3-methoxy-4-hydroxybenzaldehyde, 4-ethoxyaniline, chloroform, ethanol, DMSO, and THF were purchased from Merck (Germany). Ethidium bromide (EB), calf thymus DNA (CT-DNA), pBR322 DNA, $(Bu)_4NF$, $(Bu)_4NBr$, $(Bu)_4NI$, $(Bu)_4NCN$, $(Bu)_4NSCN$, $(Bu)_4NClO_4$, $(Bu)_4NHSO_4$, $(Bu)_4NCH_3COO$, $(Bu)_4NH_2PO_4$, $(Bu)_4NN_3$ and $(Bu)_4NOH$ were purchased from Sigma (USA). The Tris–HCl buffer solution was prepared with triple-distilled water. CT-DNA stock solution was prepared by diluting DNA to Tris–HCl/NaCl buffer (5 µM Tris–HCl, 50 µM NaCl, pH 7.2), and kept at 4 °C for no longer than two days.

Synthetic Procedures

(*E*)-4-[(4-Ethoxyphenylimino)methyl]-2-methoxyphenol 3-Methoxy-4-hydroxybenzaldehyde (0.01 mol) was added to a dry THF (100 mL) solution of 4-ethoxyaniline (0.01 mol). The mixture was stirred and heated for 2 h. The title compound was obtained from the evaporation of THF. It was crystallized from chloroform/*n*- heptane as a light yellow crystal, m.p. 104 °C, 2.44 g (90%) yield. $C_{16}H_{17}NO_3$ (271.31): Calcd. C 70.76, H 6.27, N 5.16; found C 70.73, H 6.26, N 5.16. IR (KBr): ν/cm^{-1} = 3446 s (Ar–OH stretch), 3156m, 3083m, 3058 m (Ar-H stretch), 2981 m, 2939 m, 2881 m, 2835 m (C-H stretch), 1618 s (C=N stretch), 1606 s, 1589 s (C=C stretch), 1560 s, 1508 s (C-H scissoring and bending), 1308 s, 1213 s, 1051 s (Ar–OC_2H_5 + Ar–OCH_3 symmetrical stretch).

X-Ray Crystallography and Data Collection

Crystallographic data were recorded on a Bruker Kappa APEXII CCD area-detector diffractometer using MoK_α radiation (λ = 0.71073 Å) at T = 100 K. Data collection, reduction, and corrections for absorption and crystal decomposition for compound were achieved by using X-AREA, X-RED software.[28] The crystal structure was solved by SHELXS-97 and refined with SHELXL-97.[29,30] The positions of the H atoms bonded to C atoms were located geometrically and refined as riding with a respective C-H distance of 0.93 Å corresponding to the aromatic C-H bonds. All atoms (except hydrogen) were located from a difference Fourier map and refined anisotropically. The details of the X-ray data collection, structure solution, and structure refinements are given in Table 1. The bond distances, bond, and torsion angles are listed in Table S1 (supplementary materials). The molecular structure with the atom-numbering scheme is shown in Figure 1.[31] Crystallographic data (excluding structure factors) for the structures reported in this paper has been deposited with the Cambridge Crystallographic Data Centre as supplementary publication number CCDC 1048672.

DFT Calculation Details

The theoretical calculations of the title compound were performed by using the Gaussian 09 software package program.[32] The input and output files were visualized via GaaussView 5 visualization program.[33] The geometry optimization, structural properties, vibration spectra and NLO properties of the title compound were determined through the applications of B3LYP (Becke's three-parameter hybrid model using the Lee–Yang Parr correlation[34,35] with the 6-311++G(d,p) basis set.[36]

Table 1. Crystallographic and structure refinement data for the title compound

Chemical formula	$C_{16}H_{18}NO_3$
Crystal shape/color	Prism/Yellow
Crystal size (mm^3)	0.20 × 0.24 × 0.32
Formula weight	272.31
Crystal system	Monoclinic
Space group	*P21/c*
a (Å)	10.312(1)
b (Å)	9.995 (1)
c (Å)	26.5762(4)
β (°)	92.276(1)
Volume ($Å^3$)	2737.01 (6)
Z	8
D_x ($Mg\ m^{-3}$)	1.317
μ (mm^{-1})	0.091
F_{000}	1152
Radiation/ T(K)	MoK_α (λ = 0.71073 Å) / 108(2)
Diffractometer/meas.meth scans	Bruker APEX-II CCD / *w* and *φ*
Absorption correction	Multi-scan
T_{min}	0.9700
T_{max}	0.9785
No. of measured/independent/observed reflections	25331 / 6766 / 4775
h	−13 to 13
k	−11 to 13
l	−30 to 35
Criterion for observed reflections	$I > 2\sigma(I)$
θ_{min} / θ_{max}	1.53 / 28.25
$R\ [F^2 > 2\sigma(F^2)]$, *wR*, *S*	0.0455, 0.1012, 1.025
No. of parameters	367
Weighting scheme	$w = 1/[\sigma^2(F_0^2) + (0.0694P)^2]$ $P = (F_0^2 + 2F^2)/3$
$\Delta\rho_{max}$, $\Delta\rho_{min}$ ($e\ Å^{-3}$)	0.283, −0.244

The optimized structure parameters of the title compound were also calculated by using Hartree-Fock (HF) using the 6-311++G(d,p) basis set. The potential energy surface scans (PES) for the conformational analysis of the compound were obtained by minimizing the potential energy using B3LYP/6-311++G(d,p) level of theory for all geometrical parameters by varying the torsion angles in steps of 10° in the range of 0°–360° rotation around the bond. Moreover, a detailed assignment of vibrational modes for the title compound was performed on the basis of potential energy distribution (PED) by using VEDA 4 program[37] based on the B3LYP/6-311++G(d,p) level. ^1H NMR and ^{13}C NMR chemical shifts were calculated within GIAO approach[38] which is one of the most common approaches for calculating nuclear magnetic shielding tensors. To investigate the reactive sites and to identify sites of intra- and inter-molecular interactions of the compound, molecular electrostatic potential surface was evaluated by using B3LYP/6- 311++G(d,p) level. The total molecular energies, HOMO and LUMO energies and HOMO- LUMO band gaps were predicted by the same level. For the title compound, the chemical hardness (*η*) was calculated by using HOMO and LUMO energies.[39] Finally, The total molecular dipole moment (μ_{tot}), linear polarizability (α_{ij}), and the first-order

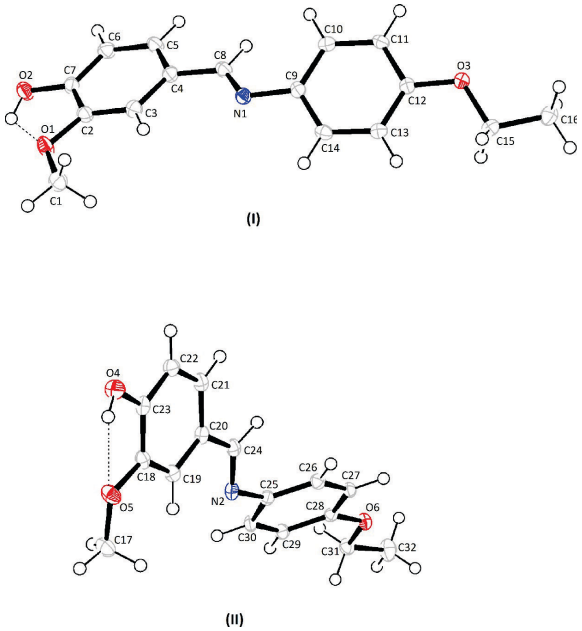

Figure 1. *Ortep-3* diagram of the title compound. The intermolecular hydrogen bond is shown as a dashed line.

hyperpolarizability (β_{ijk}) was predicted by the B3LYP method with same base sets 6-311++G(d,p) for NLO properties. Thanthiriwatte and Nalin de Silva were explained in detail previously that how is the calculations of the total dipole moment (μ_{tot}), linear polarizability (α_{ij}), and the first-order hyperpolarizability (β_{ijk}) from the Gaussian output file.[40]

Molecular Docking Calculations

Molecular docking calculations were performed on AutoDock-Vina software[41] and AutoDockTools (ADT) was used for creating docking data entry files. The polar hydrogens and Kollman atomic charges were added to the target feruloyl esterase by used ADT graphical. Water molecules and co-crystallized ligands were removed with Discover Studio Visualizer 4.0. The (*E*)-4-[(4-ethoxy-phenylimino)methyl]-2-methoxyphenol was prepared for docking by minimizing its energy at B3LYP/6-311++G(d,p) level. ADT was performed to add partial charges by Geistener method and to define torsions and rotatable bonds. The active site of the receptor was defined to include residues of active site within the grid size of 40Å x 40Å x 40Å for FEA enzyme and 20Å x 20Å x 30Å for A-DNA and B-DNA protein. Receptor-ligand interactions were demonstrated with PyMol and Discover Studio Visualizer 4.0 software.[42,43]

Screening for Antimicrobial Activities

Bacillus subtilis ATCC 6633, *Staphylococcus aureus* ATCC 25923, *Escherichia coli* ATCC 25922, *Enterococcus faecalis* ATCC 29212, *Pseudomonas aeruginosa* ATCC 27853, *Escherichia coli* NRRL B-3704, *Proteus vulgaris* ATCC 13315, *Candida albicans* ATCC 60193, and *Candida tropicalis* ATCC 13803 were used as microorganisms. Ampicillin and fluconasol were used as controls in this study as they are well-known broad-spectrum antibiotics that have different mechanisms of activity, such as inhibition of cell wall synthesis (ampicillin).[44] MIC was evaluated by broth microdilution test. The test compounds were prepared by dissolving in a minimal volume of DMSO and were serially diluted in Mueller-Hinton broth at concentrations in the range of 1–500 µg/mL. Inoculated plates were incubated at 37 °C and results evaluated after 24 h for bacteria and 48 h for fungi.

DNA-Binding Experiments

The UV-Visible spectra titrations were carried out in Tris–HCl/NaCl buffer at room temperature to investigate the binding affinity between CT-DNA and the Schiff base. The UV-Vis absorbance at 260 and 280 nm of CT-DNA solution in Tris buffer gives a ratio of 1.8–1.9, indicating that the DNA was sufficiently free of protein. [45] Tris–HCl/NaCl buffer (3 mL) and the solutions of Schiff base of buffered CT-DNA solution was added to each cuvette in order to eliminate the absorbance of DNA itself. Before the absorption spectra were recorded, the Schiff base-DNA solutions were incubated at room temperature for 5 min.

Anion Sensors Measurements

Schiff base (0.006 mmol) was dissolved in DMSO (50 mL). Tetrabuthylammonium salts (F^-, Br^-, I^-, CN^-, SCN^-, ClO_4^-, HSO_4^-, CH_3COO^-, $H_2PO_4^-$, N_3^-, OH^-) (0.006 mmol) were dissolved in DMSO (50 mL). Each solution of tetra-butylammonium salts was added to the Schiff base solution (1:1) in the UV cuvette and tube. After mixing them, UV absorption spectra and photographs were taken at room temperature.

RESULTS AND DISCUSSION

Description of the Crystal Structure

The title compound, with an *Ortep-3* view shown in Figure 1, crystallizes in the monoclinic space group *P21/c* with *Z* = 8 in the unit cell. The asymmetric unit of the title compound contains two independent molecules, namely (I) and (II). The molecules (I) and (II) in the asymmetric unit are non-planar. The dihedral angles between the two phenyl ring systems [part 1:C2−C8, C1, O1, O2 for (I), C18−C24, O4, O5 for (II); part 2: N1, O3, C9−C16 for (I), N2, O6 C25−C32 for (II)] are 30.6(1)° and 49.2(3)°, respectively, for molecules (I) and (II). In the azomethine groups, the N1–C8 distance is 1.282(2) Å for molecule (I) and N2−C24 distance is 1.284(2) Å for molecule (II). The bond lengths and bond angles of the

title compound are in a good agreement with those of the related structures.[39,46–50] For example, the double distance of N–C is 1.299(2) Å for 1-[(4-ethoxyphenylimino)methyl]napthalene-2-ol.[50] In the crystal structure of the title compound, there are two intramolecular and fifteen intermolecular hydrogen bonds. The donor and acceptor distances are 2.677(1) Å for O2– H2···O1 and 2.714(1) Å for O4–H4···O5 for the intramolecular hydrogen bonds, respectively Table S2, Figures 1 and S1.

X-Ray structure determinations reveal that the enol tautomer is favoured over the keto tautomer. This is evident from the observed O2–C7 bond distance of 1.353(2) Å and O4–C23 bond distance of 1.354(2) Å, which is consistent with the O–C single bond; similarly the N1– C8 distance of 1.282(2) Å and the N2–C24 distance of 1.284(2) Å are also consistent with the N=C double bonding, respectively. The average single O–C is 1.366(2) Å for similar to investigated compound structure of 1-[(4-ethoxyphenylimino)methyl]napthalene-2-ol.[50]

Optimized Molecular Structure

The calculated bond distances, bond angles, and selected torsion angles are compared with the experimental values of the title compound (Table S1). The conformational discrepancies between the X-ray structure and optimized counterparts by using Hartree-Fock (HF), and the B3LYP functional with 6-311++G(d,p) basis set can be seen in Figure S2a and S2b. As seen from Figure S2a and S2b, when the X-ray structure of the title compound is compared with its optimized counterparts, slight conformational discrepancies are observed between them. The most significant structural disparities are found in the orientation of 3-methoxy-4-hydroxybenzaldehyde ring (part 1) in the compound. This structural disparity is defined by torsion angles C9–N1–C8–C4 [177.55(13)°], C8–N1–C9–C14 [-153.23(13)°] and C8–N1–C9–C10 [26.3(2)°] for experimental values. These torsion angles are the orientation of the aldehyde ring (part 1) part with respect to the 4-ethoxyaniline ring (part 2) part, and have been calculated for the investigated compound as 178.525, -141.814, 40.709° for the HF/6-311++G(d,p) level and 177.192, -148.042 and 34.471 for the B3LYP/6-311++G(d,p) level. Part 1 and part 2 are inclined at the angle of 30.6(1)° for (I) and 49.2(3)° for (II) with respect to one another experimentally, whereas this angle has been calculated as 36.4(3)° for the B3LYP/6-311++G(d,p) level and 41.9(3)° for the HF/6-311++G(d,p) level.

The bond lengths of C8–N1 [1.282(2) Å] and C24–N2 [1.284(2) Å] have a double bond character. These bond lengths are predicted by the bond lengths of 1.254 Å for HF and 1.279 Å for the B3LYP level.

It is well known that DFT-optimized bond lengths are usually longer and more accurate than HF due to the inclusion of electron correlation. [50,51] According to our calculations, the biggest difference between experimental and calculated bond lengths is about 0.032 Å for HF and 0.056 Å for B3LYP level, while the root means square error (RMSE) is found to be 0.012 Å for HF and 0.014 Å for B3LYP. According to the RMSE value, the bond lengths obtained by the B3LYP level show a good correlation with the experimental values. For bond angles, the opposite was observed. As can be seen from Table S1, both the biggest difference and the RMSE for the bond angles obtained by the DFT calculations (B3LYP level) are larger than those determined by HF. A logical method for globally comparing the structures obtained from theoretical calculations is by superimposing the molecular skeleton on that obtained from X-ray diffraction. According to these results, it may be concluded that the B3LYP calculation reproduces the bond lengths well, while the HF method is better at predicting the bond angles and 3D geometry of the title compound. Whereas the most of the calculated bond lengths are slightly longer than the experimental values, as seen from Table S1, the calculated bond lengths and angles are in good agreement with the experimental values for the title compound and also similar compounds in the literature.[39,46-50]

We noted that the experimental results belong to the solid phase whereas theoretical calculations belong to the gas-phase. The result in the differences of bond parameters between the calculated and experimental values depend on the existence of the crystal field along with the inter-molecular interactions connects the molecules together in the solid state.[50]

Potential Energy Surface (PES) Scan

It will be interesting to investigate if the conformation obtained by optimization of the molecule in the crystal structure is just a local minimum, or it is indeed the most favorable molecular conformation in the vacuum. For this purpose the conformational search taking into account the single bonds C4-C8 and N1-C9 have been performed at the torsion angles T1(C5- C4-C8-N1) and T2(C8–N1-C9-C10). The scans were obtained by minimizing the potential energy using B3LYP/6-311++G(d,p) level of theory in all geometrical parameters by varying the torsion angles at a step of 10° in the range of 0–360° rotation around the bond. The variations of potential energy change from its equilibrium with the torsional perturbation are presented in Figure 2a and 2b. Potential energy surface (PES) scan for torsion angles T1 shows only one minima positions at 180°, while T2 shows four minima positions at 30°, 150°, 210° and 330°. The minima of the curves correspond to the low energy conformers which are most highly populated and usually responsible for chemical and biological properties of the molecule. These energies of the most stable conformation are −900.58771 Hartree for T1 and −900.58768 Hartree for T2.

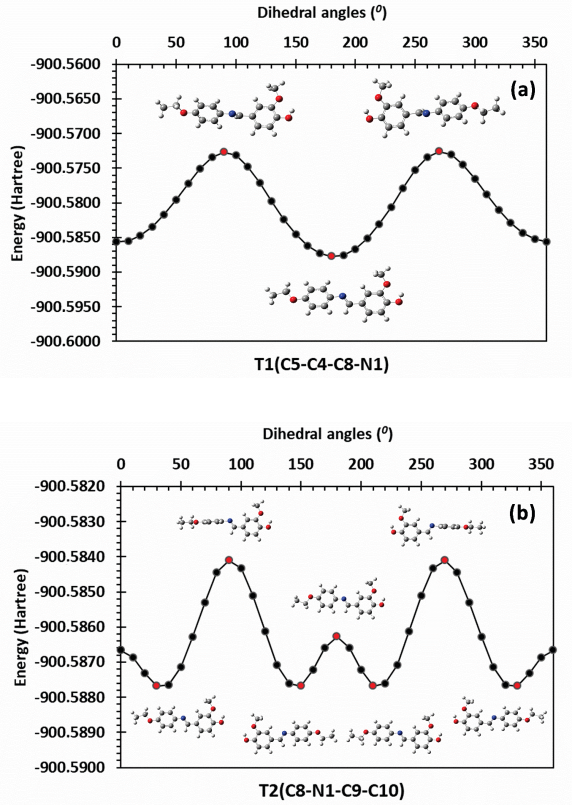

Figure 2. Potential energy curves calculated at B3LYP/6-311++G(d,p) level for the investigated molecule along the torsion angles **(a)** T1(C5–C4–C8–N1) and **(b)** T2(C8–N1–C9–C10).

Molecular Electrostatic Potential (MEP)

MEP has been used to explain and predict relative reactivity sites for the electrophilic and nucleophilic attack, investigation of hydrogen bonding interactions, molecular cluster and crystal behavior and the correlation and prediction of a wide range of macroscopic properties.[51]

MEP in the B3LYP/6-311G++(d,p) optimized geometry was determined. MEP is shown in Figure 3. The negative (red) and the positive (blue) regions in the MEP were related to electrophilic reactivity and nucleophilic reactivity, respectively. Title molecule has several possible sites for electrophilic attack. Negative electrostatic potential regions (red color) are mainly localized over the oxygen atoms. The negative MEP value is −0.032 a.u. for O2 atom. The deepest positive point of MEP is localized on the etheric ArOH, $ArOCH_2CH_3$ and $ArOCH_3$ atoms and these values are almost +0.032 a.u. These sites give information about the region from where the compound can have intermolecular interactions. It can be indicative of strong intramolecular and intermolecular hydrogen bonds (O–H···N) in the crystal structure.

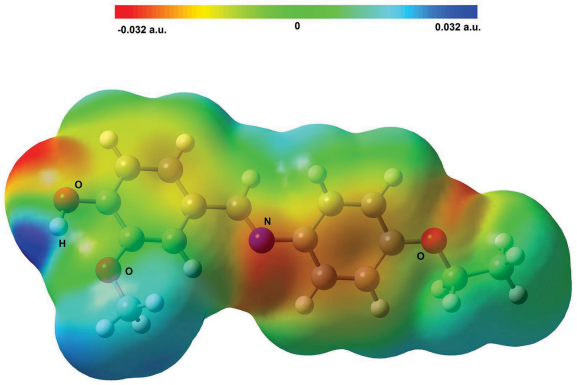

Figure 3. Molecular electrostatic potential (MEP) map calculated at B3LYP/6-311++G(d,p) level.

Natural Bond Orbital (NBO) Analysis

The double bond character of N1–C8 was revealed by NBO analysis (Table S3). The aldehyde ring (ring 2), consisting of C2, C3, C4, C5, C6, C7 atoms, and rings (ring 1) of the aniline part, consisting of C9, C11, C12, C13, C14 atoms, are typically in a single-double arrangement that forms the conjugate structure. The NBO occupancies of single O1–C2, O2–C7 and O3–C12 are at the same level in the whole molecule. The calculated results from the NBO analysis are consistent with those obtained from X-ray structure analysis of the compound. So, NBO analysis can be a very useful method for molecular modelling.

The results of second-order perturbation theory analysis of the Fock matrix at B3LYP/6-311++G(d,p) level of theory found the stabilization energies larger than 3.0 kcal/mol. The stabilization energy $E^{(2)}$ value increases with the strong interaction between electron donors and electron acceptors. Also, the larger the stabilization energy $E^{(2)}$ values, the greater the extent of the conjugation of the whole system. The strong intramolecular hyperconjugative interaction of the σ and π electrons of C–C to the anti C–C bond of the aromatic rings results in stabilization of some part of the rings, such as the intramolecular hyperconjugative interaction of the σ(C2–C3) contributed to σ^*(C2–C7) and σ^*(C3–C4) stabilization of 4.28 and 3.40 kcal/mol. This enhanced further conjugation with antibonding orbitals π* of the C4–C5 and C6–C7 which results in strong delocalization of 16.98 and 18/56 kcal/mol, respectively. The results from the NBO analysis indicate that the C4–C5, C9–C14, C10–C11 and C12–C13 bonds have the same kind interaction.

The donor orbitals LP(2) of O3 have strongest interaction energies resulting in stabilization of 29.27 kcal/mol. This important interaction reveals the existence of intermolecular hydrogen bonding between O atom of imine ring (ring 2) and C atom of aldehyde (ring 1) (C–H···O)

in the compound. The donor orbitals LP(2) of O2 have the second strongest interaction energies resulting in stabilization of 28.85 kcal/mol, and this interaction implies the existence of intramolecular hydrogen bond. The NBO analysis provides an efficient method to study inter- and intramolecular bonding such as C–H···O and O–H···O interactions. These interactions and bonds significantly influence the crystal packing of this molecule.

Vibrational Spectra

The vibrational band assignments were performed at B3LYP/6-311++G(d,p) theory level defined from their potential energy distributions (PED) to compare the experimental (FT-IR) and calculated vibrational frequencies of the title compound (Figure S3). We analyzed the normal vibrational frequencies and compared our calculated results for the investigated compound with the experimental ones on the basis of potential energy distributions (PED) (Table S4).

It is well-known that the vibrational wavenumbers obtained by DFT computations are usually overestimated compared to their experimental counterparts. To overcome discrepancies between observed and calculated wavenumbers, the scaling factors were introduced by assuming the relationship between the calculated unscaled (ν_{ucal}) and experimental (ν_{exp}) wavenumbers are linear and described by the following equation:

$$\nu_{exp} = 0.96287\nu_{ucal} + 7.99320, \quad R^2 = 0.99664$$

According to the fitting results of equation, the general scale factor value was found to be 0.96287 for B3LYP/6-311++G(d,p) level. We calibrated the vibrational wavenumbers by using a scale factor value of 0.96287.

The infrared spectra of the title compound contain some characteristic bands for the stretching vibrations of O–H, C–H, C–H_2, C–H_3, C=N, C=C, C–C, C–O and C–OH groups.

UV-Visible Spectra and HOMO-LUMO Studies

An experimental UV–Visible spectrum of the title compound is given in Figure S4. In order to understand electronic transitions in the title compound, TD-DFT calculations were performed for different solvents (DMSO, EtOH, and chloroform). The calculated frontier orbital energies, absorption wavelengths (λ), oscillator strengths (f) and excitation energies (E) for different solvents (DMSO, EtOH, and chloroform) are listed in Table S5. The UV- Visible spectra of the title compound shows three bands at 240, 253, 336 nm and 253, 288, 340 nm for $CHCl_3$ and DMSO and, four bands at 207, 228, 284, 337 nm for Et-OH, which is assigned to the π–π* and n–π* transition of the C=C and C=N. The pictorial form of the HOMO and LUMO charge transfer is shown in Figure 4. The major contributions of the transitions were designated with the aid of GaussView 5 visualization program.[33] The visible absorption maxima of this molecule from calculations of the molecular orbital geometry due to electron transition between the calculated absorption maxima are found to be 361, 302 and 280 nm in DMSO solution, 360, 301, 253, and 244 nm in chloroform solution and 360, 301, 280, 233 and 226 nm in ethanol solution. The maximum absorption wavelength corresponds to the electronic transition from HOMO to LUMO with 68% contribution. This transition (HOMO-LUMO) confirms the π–π* and n–π* transitions. They are all assigned to the π–π* and n–π* transitions which are also confirmed by NBO analysis.

The HOMO–LUMO energy gap value was found to be 3.9203 eV at B3LYP/6- 311++G(d,p) in the gas phase. They are mostly π-antibonding type molecular orbitals in the structure. The chemical hardness is useful to rationalize the relative stability and reactivity of chemical compounds. For the title compound, the chemical hardness (η) was calculated as 1.9602 eV.

^{1}H- and ^{13}C-NMR Spectra

The calculated and experimental ^{1}H- and ^{13}C-NMR chemical shift values of the title molecule are listed in Table S6 (Figure S5). The OH and azomethine (-N=C-H) protons are observed as singlet δ = 9.5 and 8.2 ppm for the compound. The calculated values for these atoms are (in gas phase/DMSO) 5.98/8.35 and 6.03/8.52 ppm, respectively.

The observed resonance signals between δ = 6.66-7.30 ppm (multiplet) correspond to chemical shifts of the protons in aromatic rings. The calculated chemical shifts for aromatic protons are found at 7.01-8.56 ppm in the gas phase and 7.35-8.71 ppm in DMSO. The protons of ArOC$\underline{H_3}$ are observed at 3.70 ppm as a singlet, while these protons are calculated at 3.91 ppm in the gas phase and in 4.04 ppm in DMSO. The etheric ArOC$\underline{H_2}$ and ArOCH$_2$C$\underline{H_3}$ protons of the compound gave a quartet and triplet at δ = 3.6 and 1.1 ppm, respectively. The calculated values for these atoms are (in gas phase/DMSO) 3.86/1.44 and 4.01/1.47 ppm, respectively.

According to the proton decoupled ^{13}C NMR spectra, the compound has 14 signals. The aliphatic Ar$\underline{C}$H=N-Ar, $\underline{C}H_3$O-Ar, $CH_3\underline{C}H_2$O-Ar and $\underline{C}H_3CH_2$O-Ar carbons are observed at δ = 161.9, 63.63, 55.97 and 15.17 ppm for the compound, the calculated chemical shift values for these carbon's in gas phase/DMSO is found at 159.93/162.30, 55.45/56.04, 65.73/66.23, 15.62/15.42 ppm, respectively. The carbon-13 NMR isotropic chemical shift values of carbon atoms in phenyl and naphthalene aromatic rings, except these mentioned carbon atoms, are experimentally given resonance signals at the interval 110.69–158.4 ppm.

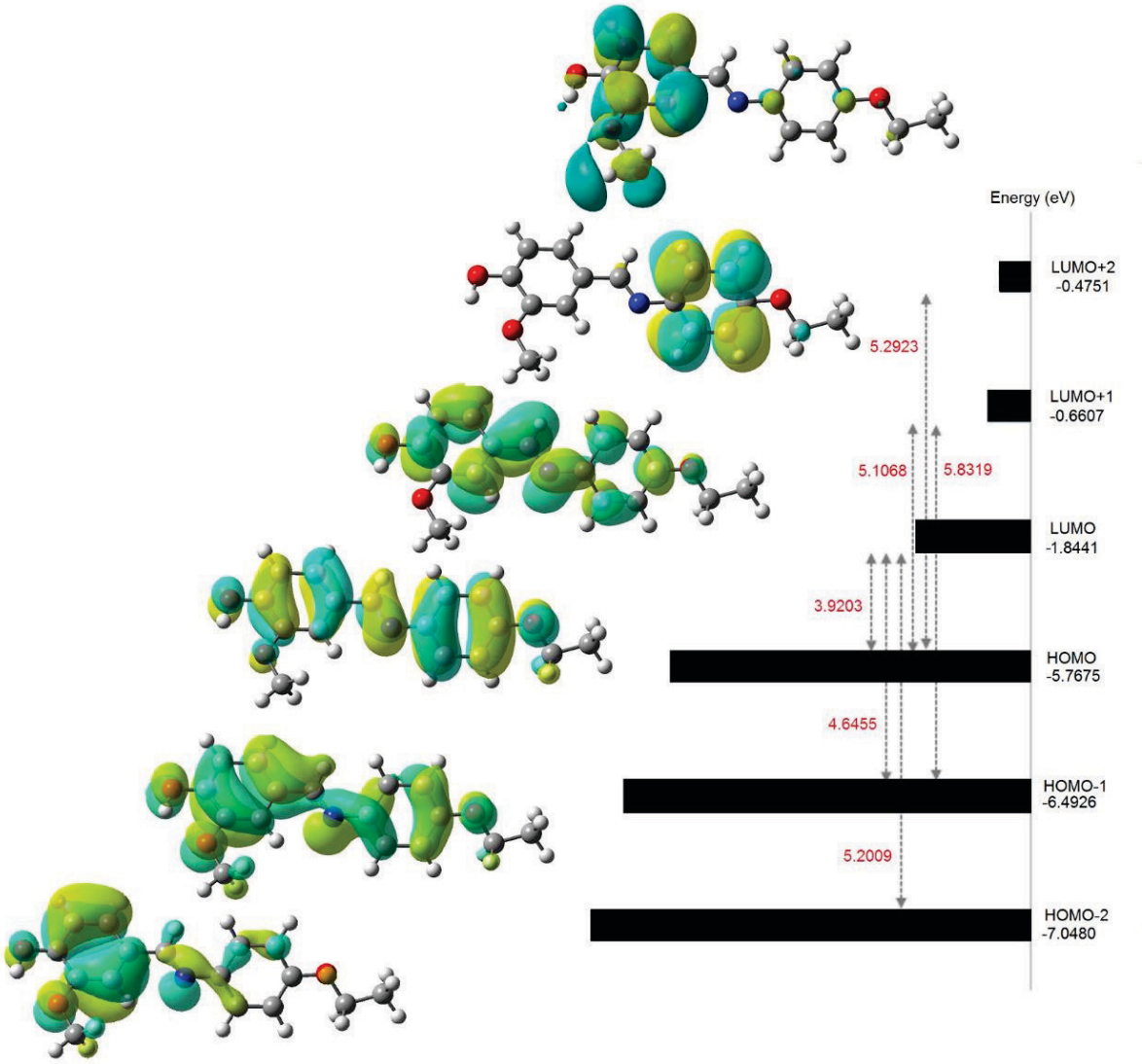

Figure 4. Molecular orbital surfaces and energy levels for the HOMO, HOMO-1, LUMO, and LUMO+1 of the title compound computed at B3LYP/6-311++G(d,p) level.

The chemical shifts δ/ppm: 158.4 (s, C1, Cipso-, CH_3CH_2-O-), 150.4 (s, C7, Cipso-, CH_3-O-), 149.5 (s, C8, Cipso-, HO-), 145.0 (s, C4, Cipso, -N=CH-), 128.7 (s, C5, Cipso, -CH=N-), 125.1 (s, C10, C-phenyl), 123.3 (s s, C3, C-phenyl), 115.8 (s, C9, C-phenyl), 115.3 (s, C2, C-phenyl), 110.69(s, C6, C-phenyl), while the computed chemical shift values in gas phase/DMSO for these carbon atoms are in the regions 109.28–164.72ppm/109.12–164.91ppm.

In conclusion, X-ray, FT-IR, Quantum Chemical Calculations, UV–Visible, ^{1}H- and 13C-NMR results show that the compound exists in the enol-imine form.

Non-Linear Optical Effects

The NLO properties such as the total dipole moment (μ_{tot}), linear polarizability (α_{ij}), and the first hyperpolarizability (β_{ijk}) of the title molecule were also investigated in this study. It is well known that the higher values of molecular linear polarizability and first hyperpolarizability are important for more active NLO properties. The polarizabilities and hyperpolarizability are reported in terms of atomic units (a.u) and the calculated values have been converted by using 1 a.u^3 = (0.529)^3 Å^3 for α and 1 a.u = 8.641 × 10^{-33} cm^5/esu for β.

The total dipole moment (μ_{tot}), the linear polarizability (α) and the first hyperpolarizability (β) were calculated at the B3LYP/6-311++G(d,p) level of the compound. The calculated total dipole moment (μ_{tot}), polarizability (α) and first hyperpolarizability (β) for the title compound are 3.0618 Debye, 36.8044 Å^3, and 8.2446 × 10^{-30} cm^5/esu, respectively. These α values are approximately

Table 2. MIC (μg/mL) of the compound

Microorganisms	Compound	Antibiotic	
	Schiff base	Ampicilin	Fluconasol
S. aureus ATCC 25923	128	1	-
E. faecalis ATCC 29212	128	2	-
B. subtilis ATCC 6633	128	1	-
E. coli ATCC 25922	256	16	-
E. coli NRRL B-3704	128	32	-
P. aeruginosa ATCC 27853	128	2	-
P. vulgaris ATCC 13315	128	2	-
C. albicans ATCC 60193	< 0.25	-	1
C. tropicalis ATCC 13803	32	-	2

1.6 times greater than that of *para*-nitroaniline (*p*-NA) molecule, which is a typical NLO material.[52,53] *p*-NA molecule was chosen as a reference molecule because there were no experimental values about the title complex in the literature. Urea is also one of the most widely used molecules for determination of NLO properties of molecular systems and can be used as a reference molecule in NLO studies. The calculated values of urea at B3LYP/6-311++G(d,p) level were found to be 4.90 Å^3 for α and 0.781 × 10^{-30} cm^5/esu for β. The polarizability and first hyperpolarizability for the title compound is approximately 7.5 and 10.6-fold larger than those of urea when our results are compared to those for pNA and urea. When it is compared with the similar Schiff base ligands in the literature, the calculated values of first hyperpolarizability (β) in the compound are smaller than that of 1-[(4-et-hoxyphenylimino)methyl]napthalene-2-ol (33.2309 × 10^{-30} cm^5/esu),[50] (*E*)-4-[(pyridin-3-ylimino)-methyl]benzene-1,3-diol (16.432 × 10^{-30} cm^5/esu)[54] calculated with B3LYP/6-311++G(d,p) method and greater than that of *N*-(2,5-methylphenyl)salicylaldimine (3.752 × 10^{-30} cm^5/esu),[55] (*E*)-2-ethoxy-4-[(4-ethoxyphenylimino)methyl]-phenol (7.0934 × 10^{-30} cm^5/esu).[39]

Minimum Inhibitory Concentration (MIC)

The data reported in Table 2 are the average data from three experiments. It can be observed from Table 2 that the antimicrobial results for the Schiff base have a high antifungal effect on *C. albicans* ATCC 60193, while it has a low effect on *C. tropicalis* ATCC 13803. Likewise, it has stronger antibacterial effect against *S. aureus* ATCC 25923, *E. faecalis* ATCC 29212, *B. subtilis* ATCC 6633, *E. coli* NRRL B-3704, *P. aeruginosa* ATCC 27853 and *P. vulgaris* ATCC 13315 compared to *E. coli* ATCC 25922. The highest antimicrobial effect was on *C. albicans* ATCC 60193 compared to other microorganisms. The compound differs significantly in its activity against tested microorganisms. This difference may be attributed to the fact that the cell wall in Gram-positive bacteria are of a single layer, whereas the Gram-negative cell wall is a multilayered structure, and the yeast cell wall is quite complex. Some *C. albicans* species have shown resistance to antifungal drugs. Antibacterial and antifungal activities of the compound were compared with those of the standard drugs ampicillin and fluconasol. However, it had similar or much less activity against the tested organisms except *C. albicans* ATCC 60193 compared with the reference drugs. Surprisingly, the compound had very strong effect against *C. albicans* ATCC 60193. The low activity of the Schiff base is due to their low lipophilicity, because of which penetration of the complex through the lipid membrane was decreased and hence, they could neither block nor inhibit the growth of the microorganism.

DNA-Binding

The potential binding ability of the compound to CT-DNA was characterized by UV spectroscopy. The absorption spectra of the Schiff base in the absence and presence of CT- DNA at different concentrations are given in Figure 5. Absorption spectroscopy is one of the most commonly used methods to investigate the effects of any material on DNA. If it has an intercalation effect against DNA, generally the hypochromic effect is observed.[56,57] But if the material's interaction with DNA is electrostatic or partially intercalative, the hyper-chromic effect is observed. Moreover, the red shift of the maximum absorptions indicates that the difference between HOMO and LUMO energy levels decreases and that the complex interacts with DNA. The absorption spectra for the Schiff base in the absence and presence of CT-DNA are shown in Figure 5. In the UV region, three intense bands were absorbed in 272, 340 and 429 nm for Schiff base. In the presence of CT-DNA, a decrease in peak intensities was observed in the absorption spectra of Schiff base. In addition to the

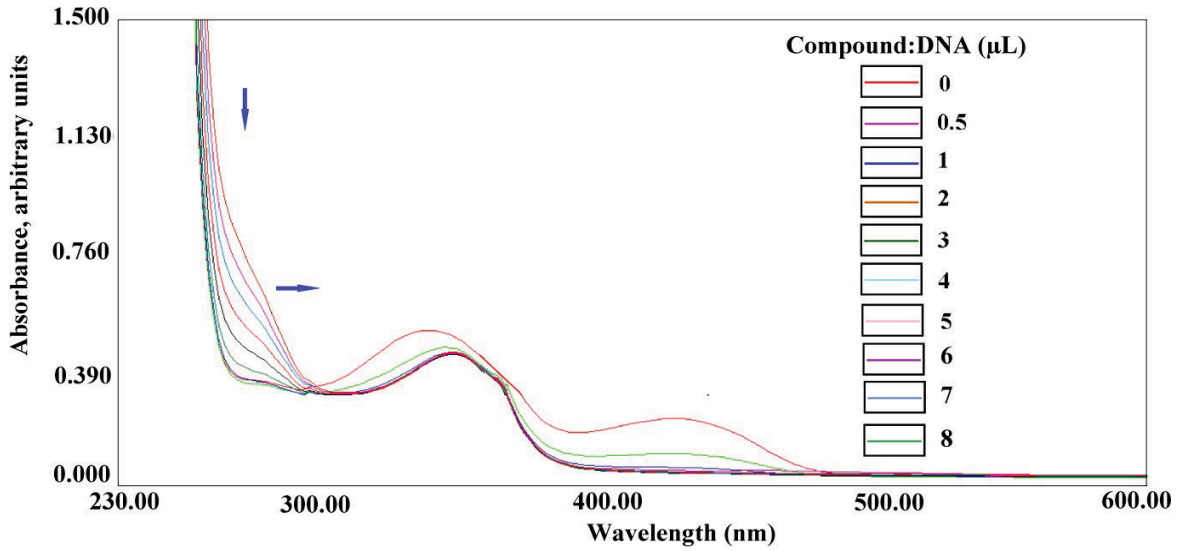

Figure 5. Absorption spectra of the compound in the absence and presence of increasing amounts of CT-DNA at room temperature in Tris–HCl/NaCl buffer (pH 7.2).

increase in intensity, a small red shift (bathochromism; 6-8 nm) was also observed in the spectra for the Schiff base. The absorption bands of Schiff base at 280 nm are shown with increasing CT-DNA (0, 0.5, 1, 2, 3, 4, 5, 6, 7 and 8 µL) (Figure 5). The extent of red shift and hypochromism are commonly found to correlate with the intercalative binding strength. The Kb value obtained for Schiff base was 9.19 M^{-1}. Consequently, the observation of hypochromic effect in the absorption spectra implies that the Schiff base established an intercalative bond with DNA.

Colorimetric Anion-Sensing

In Schiff bases,[26,27,58,59] the acidic phenol proton would deprotonate upon exposure to nucleophiles and therefore, the intramolecular proton transfer occurs to the keto-amine form. And/or phenol-imine and keto-amine tautomerism occur. This phenomenon among 'Schiff bases' is exhibited due to the tautomerism between phenol-imine and keto-amine form via six membered hydrogen transfer between the phenolic hydrogen and imine nitrogen. Consequently, the anion selectivity and electrostatic DNA binding occur.

The sensing ability of the title compound (5×10^{-6} M) was studied in DMSO. Upon the addition of 1 equiv. of each anion, only CN^- resulted in the appearance of the color, which can be attributed to the hydrogen bonds between the title compound and the anions and to the resultant charge transfer processes in the title compound. On the other hand, the addition of other anions (F^-, Br^-, I^-, SCN^-, ClO_4^-, HSO_4^-, AcO^-, $H_2PO_4^-$, N_3^- and OH^-) did not induce any color changes in the compound. Sensor (*E*)-4-[(4-ethoxyphenylimino)methyl]-2-methoxyphenol displayed visual color changes upon addition of CN^- as illustrated by the colorimetric photos (Figure 6a), taken in two different illuminations: natural light and under a hand held UV lamp. In natural light, the observed color changes were from colorless to yellow for CN^-. There was no discernible fluorescence change under the hand held long wave UV lamp as yellow for CN^- (Figure 6b). The most discernable color change in the Schiff base ligand was caused by CN^-, which demonstrated that the compound can be used to selectively detect CN^-. It is important to comment on the mechanism of cyanide anion binding to the title compound. Cyanide has much weaker hydrogen bonding ability in comparison with OH^-, F^- and AcO^- with stronger nucleophilicity toward the imine group, which results in the addition reaction of CN^- to the carbon atom of an electron deficient imine group and, subsequently, fast proton transfer of the phenol hydrogen to the neighboring nitrogen anion through an intramolecular hydrogen bond. [26,27]

Molecular Docking Study of Title Compound with FAE

Schiff base ligands have been reported as plant growth regulators, antimicrobial and antibacterial activity.[60] Prediction of Activity Spectra (PASS)[61] is an online tool which predicts different types of activities based on the structure of a compound. PASS analysis of the title compound is given in Table S7. According to the PASS analysis, to evaluate the inhibitory nature of the title compound against FAE protein, molecular docking studies were performed. High resolution 3D crystal structure of FAE was downloaded from the protein data bank (PDB ID: 1UWC).[62]

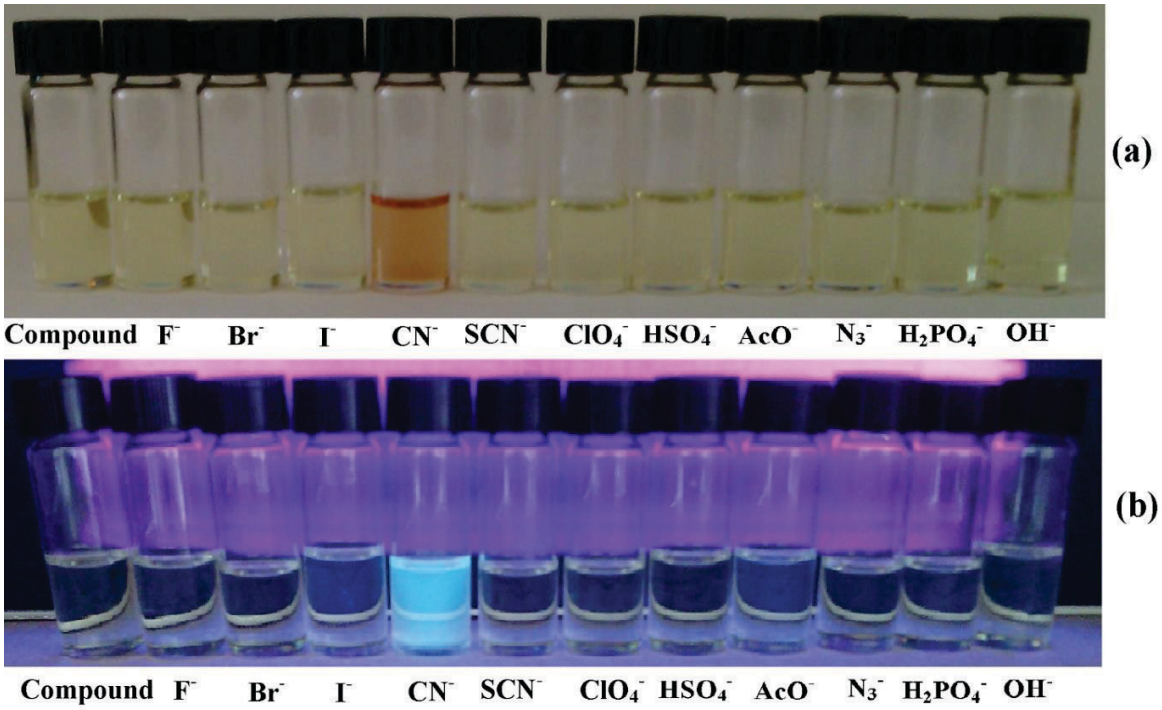

Figure 6. The color changes of the compound (1equiv) upon addition of various anions (3 equiv) of the compound under (**a**) normal light hand (**b**) hand held UV lamp (λ =365 nm).

The docking protocol we employed predicted a convenient confirmation with RMSD value well within the allowed range of 2Å. The criterion to be considered after RMSD is the bonding energy. The reason behind this priority order is that the structure may give low bonding energy outside the active site as well. The predicted bonding energy as a result of molecular docking and RMSD values are given comparatively in Table 3. Amongst the docked conformations of the title compound, the conformation which was close to the conformation of co-crystallized ligand and scored well was visualized and is given in Figure S6. Energetically the most favorable docked structure obtained from the rigid molecular docking of the title ligand with FAE is shown in Figure S7. The relative binding energy of the docked ligand-FAE is found to be −6.5 kcal/mol. The title compound binds at the active site of the FAE by weak non-covalent interactions, most prominent of which are H-bonding (3.04 Å: N atom of SER7 and O3 atom of ligand), two carbon hydrogen bond (3.65, 3.31 Å), two π-alkyl (3.85, 4.74 Å) and van der Waals interactions as shown in Figure 7. According to the calculations, the title compound might inhibit FAE.

Molecular Docking Study of the Title Compound with DNA

To understand the drug-DNA interaction molecular docking is used. Structurally different molecules bind with DNA in a different fashion, respectively. Molecular docking studies were performed to understand the interaction mechanism between the investigated compound A-DNA (PDB ID: 3V9D) and B-DNA (PDB ID: 1BNA), and the preferred molecular orientation in A-DNA and B-DNA. The predicted bonding energy as a result of molecular docking and RMSD values are given comparatively in Table 3. Energetically the most favorable docked structures obtained from the rigid molecular docking of the title compound with 3V9D (A-DNA) and 1BNA (B-DNA) are shown in Figure S8a and S8b. The relative binding energies of the docked compound-(A-DNA) and compound-(B-DNA) are found to be the same value of −6.2 kcal/mol. The compound binds at the active site of the 3V9D for A-DNA nucleic acid by weak non-covalent interactions most prominent of which are conventional H-bonds and π-alkyl interaction, while the title compound binds at active site of 1BNA for B-DNA nucleic acid by weak non-covalent interactions most prominent of which are CH···O interactions π-donor interactions and π-π interaction. These interactions are illustrated in Figure S9a and S9b. The resulting docked pose of compound-(A-DNA) complex reveals that oxygen atom (O3) of $ArOCH_2CH_3$ (part 2) binding on the surface of the DNA is involved in hydrogen bonding (2.98 Å) with the nitrogen atom (N4) of cytosine (B:DC4:N4). The nitrogen atom (N1) of compound's azomethine binding on the surface of the A-DNA is also involved in hydrogen bonding

Table 3. Binding affinity and RMSD values of different poses of the title compound as predicted Autodock Vina

Compound-inhibitor	Mode	Affinity l.b. (Å)	Distance from best mode (kcal/mol) RMSD u.b. (Å)	RMSD
Compound-(FAE)				
	1	−6.4	0.000	0.000
	2	−6.4	2.007	2.588
	3	−6.1	5.437	9.720
	4	−6.0	4.669	9.966
	5	−6.0	1.565	2.330
	6	−5.9	3.963	5.603
	7	−5.8	5.017	8.125
	8	−5.8	28.005	29.882
	9	−5.8	5.303	7.481
Compound-(A-DNA)				
	1	−6.2	0.000	0.000
	2	−6.1	1.759	8.524
	3	−6.1	4.933	6.974
	4	−6.0	1.933	8.528
	5	−6.0	2.407	3.902
	6	−5.9	2.004	2.967
	7	−5.8	2.549	4.000
	8	−5.8	1.706	2.585
	9	−5.7	1.008	2.221
Compound-(B-DNA)				
	1	−6.2	0.000	0.000
	2	−6.0	1.594	2.913
	3	−5.6	1.720	8.727
	4	−5.6	11.681	12.407
	5	−5.5	12.081	13.685
	6	−5.5	1.352	8.444
	7	−5.4	1.363	2.071
	8	−5.4	2.004	8.527
	9	−5.3	1.213	2.470

(3.23 Å) with the nitrogen atom (N6) of adenosine (A:DA8:N6). π-alkyl interaction (4.68 Å) between carbon atom of ligand and cytosine (B:DC3) and carbon hydrogen bond interaction (3.30 Å) between carbon atom of ligand and guanosine of A-DNA (A:DG5:OP2) are also present, while three carbon hydrogen bond interactions (3.64 Å) between carbon atom of ligand and cytosine of B-DNA (B:DC23:O2), (3.63 Å) between carbon atom of ligand and cytosine of B-DNA (B:DC21:O2) and (3.68 Å) between carbon atom of ligand and thymine of B-DNA (B:DT20:O2) and two π-donor interactions (3.80 Å) between phenyl group of ligand and N2 atom of guanosine (B:DG22:N2) and (3.96 Å) phenyl group of ligand and N2 atom of guanosine (A:DG4:N2), and π-π interaction (5.47 Å) phenyl group of ligand and guanosine (A:DG4) for B-DNA into the DNA grove (Figure S9a and S9b). From these results, it can be said that the title compound might inhibit the DNA.

CONCLUSIONS

The synthesis of a Schiff base (*E*)-4-[(4-ethoxyphenylimino)methyl]-2-methoxyphenol was reported. The molecular structure of the Schiff base was confirmed using the spectroscopic and crystallographic method. In addition, density functional modelling studies of the Schiff base ligand were reported in this study. The calculated geometric parameters according to the Hartree-Fock (HF) and density functional theory (DFT) with the 6- 311++G(d,p) basis set are in good agreement with the X-ray structure. The theoretical evaluation of NLO properties yielded that the title compound had larger polarizability and hyperpolarizability values than urea, which denotes its use in potential NLO applications. The potential energy surface (PES) scans two torsion angles are performed by using B3LYP/6- 311++G (d,p) level of theoretical approximation for the compound.

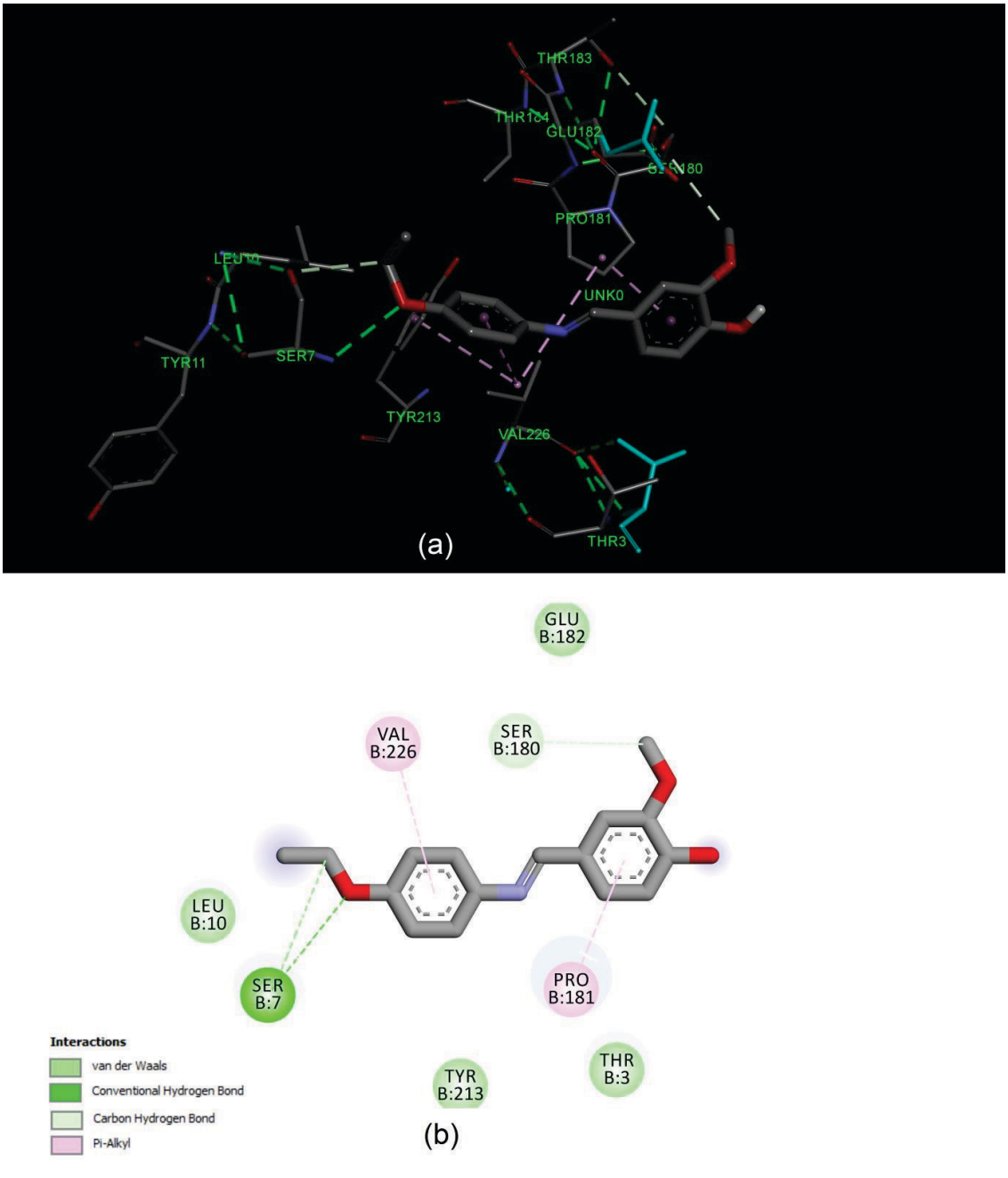

Figure 7. (a) The title compound binds at the active sites of 1UWC by weak non-covalent interactions (3D); **(b)** (2D) (For interpretation of the references to color in this figure legend, the reader is referred to the web version of this article).

As a result, quantum chemical calculations and experimental (X-ray, FT-IR, UV– Visible, ^{1}H- and ^{13}C-NMR) results show that the title compound exists in the phenol-imine form.

According to the molecular docking studies, these initial results show that the compound might inhibit FAE and DNA.

However, in this study, the compound was active against both types of bacteria, as well as active against yeasts, which may indicate broad-spectrum properties. Experimental UV–Vis spectroscopy studies of DNA binding proved that the title compound can intercalate into CT-DNA, which demonstrates its potential use as a DNA-repair agent. In addition, the compound was able to selectively recognize cyanide anions in DMSO, which was confirmed by colorimetric studies.

Acknowledgment. The authors are grateful to Ankara University Grants Commission (Project Numbers: 18H0504001) for a research grant.

Supplementary Information. Supporting information to the paper is attached to the electronic version of the article at: http://doi.org/10.5562/cca3316. Further information may be obtained from Cambridge Crystallographic Data Center (CCDC), 12 Union Road, Cambridge CB21EZ, UK, by quoting the depository number CCDC 1048672, e-mail: deposit@ccdc.cam. ac.uk.

REFERENCES

[1] N. A. Negm, N. G. Kandile, M. A. Mohamad, *J. Surfactants Deterg*. **2011**, *14*, 325.

[2] K. G. Kumar, K. S. John, R. Poduval, *J. Appl. Polym. Sci*. **2005**, *98*, 1536.

[3] Y. Zhang, X. M. Wang, L. S. Ding, *J. Serb. Chem. Soc*. **2010**, *75*, 1191.

[4] H. R. Jia, B. Kucukoz, Y. H. Xing, P. Majumdar, C. S. Zhang, A. Karatay, G. Yaglioglu, A. Elmali, J. Z. Zhao, M. Hayvali, *J. Mater. Chem.* **2014**, *C2*, 9720.

[5] A. S. Nair, R. S. Joseyphus, *Spectrochim. Acta A* **2008**, *70*, 749.

[6] J. Parekh, P. Inamdhar, R. Nair, S. Baluja, S. Chanda, *J. Serb. Chem. Soc*. **2005**, *70*, 1155.

[7] Y. M. Zhou, H. Zhou, T. S. Ma, J. L. Zhang, J. Y. Niu, *Spectrochim. Acta A* **2012**, *88*, 56.

[8] M. S. Suresh, V. Prakash, *Int. J. Phys. Sci.* **2010**, *5*, 1443.

[9] Y. Zhang, X. M. Wang, L. S. Ding, *Nucleos Nucleot. Nucl*. **2011**, *30*, 49.

[10] H. Dürr, *Angewandte Chemie* **1989**, *28*, 413.

[11] E. Hadjoudis, M. Vittorakis, I. Moustakalimavridis, *Tetrahedron* **1987**, *43*, 1345.

[12] H. Dürr, H. Bouas-Laurent, *Photochromism: Molecules and Systems*, Elsevier, Amsterdam, **1990**.

[13] H. Unver, E. Kendi, K. Guven, T. N. Durlu, *Z. Naturforsch. B* **2002**, *57*, 685.

[14] H. Unver, A. Karakas, A. Elmali, *J. Mol. Struct*. **2004**, *702*, 49.

[15] H. Unver, K. Polat, M. Ucar, D. M. Zengin, *Spectrosc. Lett*. **2003**, *36*, 287.

[16] S. A. Khan, A. A. Siddiqui, S. Bhatt, *Asian J. Chem*. **2002**, *14*, 1117.

[17] S. N. Pandeya, D. Sriram, G. Nath, E. DeClercq, *Eur. J. Pharm. Sci*. **1999**, *9*, 25.

[18] P. G. More, R. B. Bhalvankar, S. C. Pattar, *J. Indian. Chem. Soc*. **2001**, *78*, 474.

[19] N. Solak, S. Rollas, *Arkivoc* **2006**, 173.

[20] P. D. Beer, P.A. Gale, *Angew. Chem. Int. Edit*. **2001**, *40*, 486.

[21] K. W. Kulig, B. Ballantyne, *Cyanide toxicity*, US Department of Health & Human Services, Public Health Service, Agency for Toxic Substances and Disease Registry, **1991**.

[22] M. Yildiz, Z. Kilic, T. Hokelek, *J. Mol. Struct*. **1998**, *441*, 1.

[23] H. Nazir, M. Yildiz, H. Yilmaz, M.N. Tahir, D. Ulku, *J. Mol. Struct*. **2000**, *52*, 241.

[24] S. Dalapati, S. Jana, N. Guchhait, *Spectrochim. Acta A* **2014**, *129*, 499.

[25] L. B. Zang, D. Y. Wei, S. C. Wang, S. M. Jiang, *Tetrahedron* **2012**, *68*, 636.

[26] M. Yıldız, Ö. Karpuz, C. T. Zeyrek, B. Boyacıoglu, H. Dal, N. Yıldırım, N. Demir, H. Ünver, *J. Mol. Struct*. **2015**, *1094*, 148.

[27] B. Barare, M. Yildiz, G. Alpaslan, N. Dilek, F. Unver, S. Tadesse, K. Aslan, *Sensor Actuat. B-Chem*. **2015**, *215*, 52.

[28] S. Cie, X-AREA (Version 1.18) and X-RED32 (Version 1.04) Stoe&Cie, Darmstadt, Germany, **2002**.

[29] G. M. Sheldrick, SHELXS–97, Program for the solution of crystal structures, Univ. of Goettingen, Germany, **1997**.

[30] G. M. Sheldrick, SHELXL–97, Program for the refinement of crystal structures, Univ. of Goettingen, Germany, **1997**.

[31] L. J. Farrugia, *J. Appl. Crystallogr*. **1997**, *30*, 565.

[32] M. J. Frisch, G. W. Trucks, H. B. Schlegel, G. E. Scuseria, M. A. Robb, J. R. Cheeseman, G. Scalmani, V. Barone, B. Mennucci, G. A. Petersson, H. Nakatsuji, M. Caricato, X. Li, H. P. Hratchian, A. F. Izmaylov, J. Bloino, G. Zheng, J. L. Sonnenberg, M. Hada, M. Ehara, K. Toyota, R. Fukuda, J. Hasegawa, M. Ishida, T. Nakajima, Y. Honda, O. Kitao, H. Nakai, T. Vreven, J. A. Montgomery, J.E.P. Jr., F. Ogliaro, M. Bearpark, J. J. Heyd, E. Brothers, K. N. Kudin, V. N. Staroverov, R. Kobayashi, J. Normand, K. Raghavachari, A. Rendell, J. C. Burant, S. S. Iyengar, J. Tomasi, M. Cossi, N. Rega, J. M. Millam, M. Klene, J. E. Knox, J. B. Cross, V. Bakken, C. Adamo, J. Jaramillo, R. Gomperts, R. E. Stratmann, O. Yazyev, A. J. Austin, R. Cammi, C. Pomelli, J. W. Ochterski, R. L. Martin, K. Morokuma, V. G. Zakrzewski, G. A. Voth, P. Salvador, J. J. Dannenberg, S. Dapprich, A. D. Daniels, Ö. Farkas, J. B. Foresman, J. V. Ortiz, J. Cioslowski, D.J. Fox, Gaussian 09, Revision D.01, Gaussian, Inc., Wallingford CT, **2009**.

[33] R. Dennington, T. Keith, J. Millam, GaussView, Version 5, Semichem, Inc., Shawnee Mission, KS, **2009**.

[34] C. T. Lee, W. T. Yang, R. G. Parr, *Phys. Rev. B* **1988**, *37*, 785.

[35] A. D. Becke, *J. Chem. Phys.* **1993**, *98*, 5648.

[36] M. J. Frisch, J. A. Pople, J. S. Binkley, *J. Chem. Phys*. **1984**, *80*, 3265.
[37] J. P. Merrick, D. Moran, L. Radom, *J. Phys. Chem. A* **2007**, *111*, 11683.
[38] R. Ditchfie, *Chem. Phys. Lett*. **1972**, *15*, 203.
[39] C. T. Zeyrek, G. Alpaslan, H. Alyar, M. Yildiz, N. Dilek, H. Unver, *J. Mol. Struct*. **2015**, *1088*, 14.
[40] K. S. Thanthiriwatte, K. M. N. de Silva, *J. Mol. Struc-Theochem*. **2002**, *617*, 169.
[41] O. Trott, A. J. Olson, *J. Comput. Chem*. **2010**, *31*, 455.
[42] W. L. DeLano, The PyMOL Molecular Graphics System, San Carlos, CA, USA, **2016**.
[43] Accelrys Software Inc Discovery Studio Modelling Environment Relaser 4.0, Accelrys Software Inc, SanDiego, **2013**.
[44] F. F. Li, M. Feterl, Y. Mulyana, J.M. Warner, J.G. Collins, F.R. Keene, *J. Antimicrob. Chemoth*. **2012**, *67*, 2686.
[45] J. Marmur, *J. Mol. Biol*. **1961**, *3*, 208.
[46] A. D. Khalaji, M. Weil, K. Gotoh, H. Ishida, *Acta Crystallogr. E* **2009**, *65*, O436-U3134.
[47] A. D. Khalaji, K. Fejfarova, M. Dusek, *J. Chem. Crystallogr*. **2012**, *42*, 263.
[48] J. Li, Z. P. Liang, X. S. Tai, *Acta Crystallogr. E* **2008**, *64*, 02319-U02155.
[49] C. Albayrak, G. Kastas, M. Odabasoglu, R. Frank, *Spectrochim. Acta A* **201**3, *114*, 205.
[50] C. T. Zeyrek, N. Dilek, M. Yildiz, H. Unver, *Mol. Phys*. **2014**, *112*, 2557.
[51] J. S. Murray, K. Sen, *Molecular Electrostatic Potentials Cencepts and Applications*, Elsevier Science B.V, Amsterdam, The Netherlands, **1996**.
[52] L. T. Cheng, W. Tam, S. H. Stevenson, G. R. Meredith, G. Rikken, S. R. Marder, *J. Phys. Chem-Us*. **1991**, *95*, 10631.
[53] P. Kaatz, E.A. Donley, D.P. Shelton, *J. Chem. Phys*. **1998**, *108*, 849.
[54] H. Ünver, B. Boyacioglu, C. T. Zeyrek, D. Yolal, M. Yıldız, N. Yıldırım, N. Demir, A. Kiraz, A. Elmali, *J. Chem. Crystallogr*. **2018**, *48*, 32.
[55] C. T. Zeyrek, *J. Kor. Chem. Soc.* **2013**, *57*, 4461.
[56] S. Mahadevan, M. Palaniandavar, *Inorg. Chem.* **1998**, *37*, 693.
[57] R. Indumathy, S. Radhika, M. Kanthimathi, T. Weyhermuller, B. U. Nair, *J. Inorg. Biochem*. **2007**, *101*, 434.
[58] S. Roy, P. U. Maheswari, M. Lutz, A. L. Spek, H. Dulk, S. Barends, G. P. van Wezel, F. Hartl, J. Reedijk, *Dalton Trans*. **2009**, 10846.
[59] S. Dalapati, S. Jana, N. Guchhait, *Spect. Acta Part A: Mol. Biomol. Spect*. **2014**, *129*, 499.
[60] Y. Hamada, I. Takeuchi, Y. Ito, S. Matsui, T. Ito, *Yakugaku Zasshi,* **1981**, *101*, 633.
[61] A. Lagunin, A. Stepanchikova, D. Filimonov, V. Poroikov, *Bioinformatics,* **2000**, *16*, 747.
[62] K. E. McAuley, A. Svendsen, S. A. Patkar, K. S. Wilson, *Acta Crystallogr. D* **2004**, *60*, 878.